Journal of
Applied Research in Water and Wastewater
Journal homepage: www.arww.razi.ac.ir

Original paper

Numerical modeling of flow field in prismatic compound channels with different floodplain widths

Bahram Rezaei*, Alireza Safarzade

Department of Civil Engineering, Bu-Ali Sina University, Hamedan, Iran.

ARTICLE INFO

Article history:
Received 20 September 2016
Received in revised form 15 October 2016
Accepted 1 November 2016

Keywords:
Prismatic compound channel
Flow field
Numerical simulation
Turbulence model

ABSTRACT

In this paper an attempt has been made to study the effects of floodplains width and discharges on flow field in prismatic compound channels. A three-dimensional Computational Fluid Dynamic (CFD) model is used to predict the velocity distribution, secondary flow circulation and boundary shear stress in prismatic compound channels with various floodplains widths. The ANSYS-CFX software and three different turbulence models, κ–ε, κ–ε Explicit Algebraic Reynolds Stress Models (EARSM) and Eddy Viscosity Transport, are used to solve Reynolds Averaged Navier-Stokes equations. The results of the numerical modeling were then compared with experimental data on prismatic compound channels with 100 mm, 200 mm, 300 mm, and 400 mm floodplain widths. The study shows that all turbulence models are capable to predict the depth-averaged velocity in prismatic compound channels, fairly well. However, to compare with the velocity distribution, discrepancy between experimental data and boundary shear stress calculated by numerical modeling are high. Also only κ–ε EARSM model is able to predict secondary flow circulations.

1. Introduction

The prediction of the flow characteristics in compound channels with prismatic floodplains is a challenging task for engineers because of the three-dimensional nature of the flow. In compound channels flow in the main channel is faster than floodplains. This difference creates shear layer at the interface between the main channel and floodplains, leading to the generation of the vortices with vertical axes, as well as the secondary flow circulations with longitudinal axes, as shown by Sellin (1964), Tominaga and Nezu (1991), Ikeda (1999), Bousmar (2002), Rezaei (2006) and Rezaei and Knight (2011). Because of the presence of this shear layer and creation of momentum exchange between the main channel and floodplains, the conveyance capacity of the main channel decrease, while on the floodplains significantly increases. Wormleaton (1996) stated that the effects of this shear layer extend across the floodplain width and decreases to zero towards the floodplain wall. Myers (1978) also discovered that the effects of the shear layer were great at lower overbank flow depths and decrease as the flow depth increases.

There are two kinds of vortices that are generated at the interface between the main channel and the floodplain; one is the horizontal vortex due to shear layer of the stream wise flow, first observed by Sellin (1964), and the other is the secondary flow in the cross section due to anisotropy of turbulence, also called secondary flow of 2nd kind (*cf.* Nezu and Nakagawa ,1993), as shown in Fig. 1. These effects have been observed experimentally by Shiono and Knight (1991) and Tominaga and Nezu (1991) using Laser-Doppler Anemometer (LDA). Also those secondary flow cells numerically investigated by Naot et al (1993) using a non-linear κ–ε turbulence model and by Cokljat and Younis (1995), using Reynolds Stress Transport model. They have found a significant influence of secondary flows into momentum transfer and boundary shear stress. Pezzinga (1994) used a nonlinear κ–ε turbulence model to predict the uniform flow in a compound channel. He found that the proposed model is able to predict the secondary current, created by the anisotropy of normal turbulent stress. Cokljat (1993) used a Reynolds Stress Transport model and non-lineared κ–ε turbulence model to predict flow in open channel. He found out that the Reynolds Stress Transport (RST) model is able to predict the secondary flow cells but in contrast the non-linear κ–ε model failed to reproduce this result. Both models predicted equally well the shear stress. Flow field in trapezoidal open channel was numerically investigated by Wright et al. (2004) using κ–ε and various Reynolds stress models. They revealed that while all the models generally gave similar predictions for many features of the flow, there was a clear difference in the secondary flow characteristics. The κ–ε model failed to show any recirculation and the Reynolds stress models showed some recirculation in varying degrees.

Kang and Choi (2005) used a Reynolds stress model to simulate flow field in compound channels with vegetation on the floodplains. They show that by increasing vegetation density on the floodplains the point maximum stream wise means velocity moves to the main channel also bed shear stress on the floodplains decrease while it increases in the main channel. Jing et al. (2009) modeled flow in a meandering compound channel using the Reynolds stress model (RSM). They reviled that RSM can successfully model the velocity distribution and boundary shear stress in proposed flume.

Beaman (2010) used Large Eddy Simulation (LES) to model flow field in in-bank and over-bank channels. He showed that the LES model can accurately predict the flow characteristics, specially the distribution of secondary circulations in inbank and for over-bank channels at varying depth and width ratios. The main aim of the present work is to investigate whether or not the ANSYS-CFX software is able to predict the effects of flow depth and floodplain width on flow field in prismatic compound channels. Three turbulence models including κ–ε, Eddy Viscosity Transport Equation (EDDY) and Explicit Algebraic Reynolds Stress Model (EARSM) were chosen to model the velocity distribution, depth-averaged velocity and boundary shear stress distributions.

*Corresponding author Email: b.rezaei@basu.ac.ir

Please cite this article as: B. Rezaei, A. Safarzade, Numerical modeling of flow field in prismatic compound channels with different floodplain widths, Journal of Applied Research in Water and Wastewater, 3 (2), 2016, 260-270.

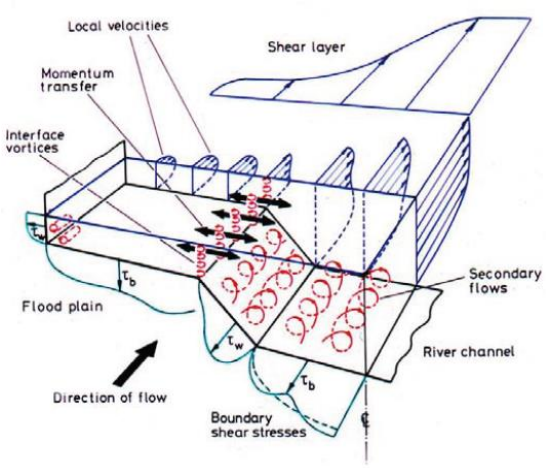

Fig. 1. Flow structure in a compound channel (Shiono and Knight. 1991).

2. Materials and methods

Experiments were carried out by Rezaei (2006), using an 18 m flume at the University of Birmingham, Department of Civil Engineering. A compound channel of simple rectangular cross-section was selected and all experiments were performed in a straight flume, almost 1200 mm in width, 400 mm in depth and with the average bottom slope of S0 = 2.003×10-3. PVC material, were used to construct rigid and smooth boundaries both for the main channel (with 398 mm width and 50 mm depth), and also for the floodplains of 400 mm wide (Rezaei. 2006). However, for experiments in prismatic compound channels, the main channel and floodplains were isolated using L-shaped aluminum sections to make different floodplain widths, 100 mm, 200 mm, 300 mm and 400 mm (see Fig. 2).

A series of three adjustable tailgates, at the downstream flume end, controlled uniform flow in compound channel. Overbank flow in prismatic compound channel tests are denoted by OPC, the first three numbers refer to the floodplain width and two code numbers denoted the flow discharge (Rezaei. 2006).

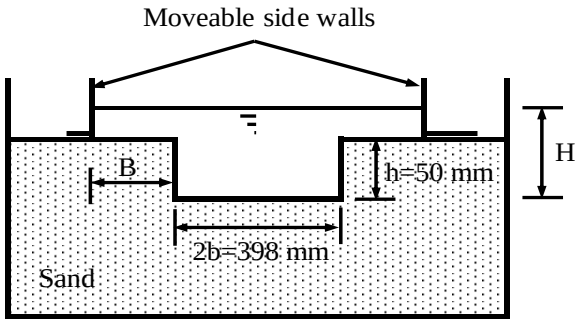

B=100 mm (OPC100) B=300 mm (OPC300)
B=200 mm (OPC200) B=400 mm (OPC400)

Fig. 2. Typical cross-section of prismatic compound channels with different floodplain widths.

2.1. Depth-averaged velocity measurement

The depth-averaged velocity distribution in a cross-section was measured at one section (14 m from the channel inlet) using a 13 mm diameter Novar Nixon miniature propeller current meter. Point depth-averaged velocity measurements were made laterally each 25 mm at a depth of 0.4*H* from the bed in the main channel and 0.4(*H* - *h*) on the floodplains (Rezaei. 2006).

2.2. Boundary shear stress measurement

Local boundary shear stress measurements were made using a Preston tube of 4.77mm outer diameter. These measurements were performed at the same sections where velocity measurements were taken. Local boundary shear stress was measured around the wetted channel perimeter at 10 mm vertical intervals on the walls and 25 mm transverse intervals on the bed.

3. Governing equations

The conservation of mass and momentum can express the flow motion. The equation for mass is called continuity equation and expressed as follows:

$$\frac{\partial \rho}{\partial t} + \frac{\partial}{\partial x_j}(\rho U_j) = 0 \quad (1)$$

in which, ρ is flow density and U_j is time-averaged components of velocity.

$$U_j = \frac{1}{\Delta t}\int_{t_1}^{t_2} u_j \, dt \quad (2)$$

Please cite this article as: B. Rezaei, A. Safarzade, Numerical modeling of flow field in prismatic compound channels with different floodplain widths, Journal of Applied Research in Water and Wastewater, 3 (2), 2016, 260-270.

The equation of motion is an expression of the second low of Newton and can be explained in the Reynolds-averaged Navier-Stokes equation,

$$-\frac{\partial P}{\partial x_i}+\frac{\partial}{\partial x_j}(\tau_{ij}-\rho\overline{u_i'u_j'})=\frac{\partial(\rho U_i)}{\partial t}+\frac{\partial(\rho U_i U_j)}{\partial x_j} \quad (3)$$

where P is pressure, τ is the molecular stress tensor (including both normal and shear components of the stress), $\rho\overline{u_i'u_j'}$ is called 'turbulent' or 'Reynolds' stresses and can be evaluated using Boussinesq Eddy Viscosity turbulence model.

$$-\rho\overline{u_i'u_j'}=\mu_T\left(\frac{\partial U_i}{\partial x_j}+\frac{\partial U_j}{\partial x_i}\right)-\frac{2}{3}\rho k\delta_{ij} \quad (4)$$

in which μ_t is the turbulence viscosity, k is the turbulence kinetic energy, and δ_{ij} is the Kronecker delta.

3.1. The κ–ε model

The standard κ–ε is classified as a two-equation model since it used two transport equations to describe turbulence (Launder and Spalding, 1974). These two transport equation are as follows:
Turbulent kinetic energy equation:

$$\frac{\partial(\rho k)}{\partial t}+\frac{\partial}{\partial x_j}(\rho U_j k)=\frac{\partial}{\partial x_j}\left((\mu+\frac{\mu_t}{\sigma_k})\frac{\partial k}{\partial x_j}\right)+P_k-\rho\varepsilon \quad (5)$$

Turbulent kinetic energy dissipation rate equation:

$$\frac{\partial(\rho\varepsilon)}{\partial t}+\frac{\partial}{\partial x_j}(\rho U_j\varepsilon)=\frac{\partial}{\partial x_j}\left((\mu+\frac{\mu_t}{\sigma_\varepsilon})\frac{\partial\varepsilon}{\partial x_j}\right)+\frac{\varepsilon}{k}(C_{s1}P_k-C_{s2}\rho\varepsilon) \quad (6)$$

where k is the turbulence kinetic energy and is defined as the variance of the fluctuations in velocity, ε is the turbulence eddy dissipation (the rate at which the velocity fluctuations dissipate), $C_{s}1$=1.44, C_{s2}=1.92, σ_k=1.00, and σ_ε=1.30 are turbulence constants. P_k is the turbulence production due to viscous forces, which is modeled using:

$$P_k=\mu_t\left(\frac{\partial U_i}{\partial x_j}+\frac{\partial U_j}{\partial x_i}\right)\frac{\partial U_i}{\partial x_j}-\frac{2}{3}\frac{\partial U_k}{\partial x_k}(\rho k+3\mu_t\frac{\partial U_k}{\partial x_k}) \quad (7)$$

For incompressible flow,($\partial U_k/\partial x_k$) is small and the second term on the right side of Equation (7) does not contribute significantly to the turbulence production.

3.2. The Eddy Viscosity Transport model

A very simple one-equation model has been developed by Menter (1997). It is derived directly from the κ–ε model and is therefore named the (κ–ε)$_{1E}$ model.

$$\frac{\partial(\rho\tilde{\nu}_t)}{\partial t}+\frac{\partial(\rho U_j\tilde{\nu}_t)}{\partial x_j}=C_1\rho\tilde{\nu}_t S-C_2\rho(\frac{\tilde{\nu}_t}{L_{vk}})^2+\left[(\mu+\frac{\rho\tilde{\nu}_t}{\sigma})\frac{\partial\tilde{\nu}}{\partial x_j}\right] \quad (8)$$

where $\tilde{\nu}$ is the kinematic eddy viscosity, $\tilde{\nu}_t$ is the turbulent kinematic eddy viscosity and C_1, C_2, and σ are model constants. The model contains a destruction term, which accounts for the structure of turbulence and is based on the Von Karman length scale:

$$(L_{vk})^2=\left|\frac{S^2}{\frac{\partial S}{\partial x_i}\frac{\partial S}{\partial x_j}}\right| \quad (9)$$

in which S is the shear strain rate tensor. The eddy viscosity is computed from:

$$\tilde{\nu}_t=\frac{\mu_t}{\rho} \quad (10)$$

3.3. Explicit Algebraic Reynolds Stress model

Explicit Algebraic Reynolds Stress Models (EARSM) represents an extension of the standard two-equation models. They are developed from the Reynolds stress transport equations and give a nonlinear relation between the Reynolds stresses and the mean strain-rate and vortices tensors. Because of the higher order terms, many flow characteristics are contained within the model without the need of solving transport equations. The implementation is based on the Explicit Algebraic Reynolds Stress model of Wallin (2000) and Wallin and Johansson (2000). The Reynolds stresses are computed from the anisotropy tensor according to its definition:

$$\overline{u_i'u_j'}=k(a_{ij}+\frac{2}{3}\delta_{ij)} \quad (11)$$

where the anisotropy tensor a_{ij} is searched as a solution of the following implicit algebraic matrix equation:

$$\begin{aligned}a=&\beta_1 S+\beta_2\left(S^2-\frac{1}{3}tra(S^2)\right)+\beta_3\left(\Omega^2-\frac{1}{3}tra(\Omega^2)\right)+\beta_4\left(S\Omega-\Omega S\right)\\&+\beta_5\left(S^2\Omega-\Omega S^2\right)+\beta_6\left(S\Omega^2+\Omega^2 S-\frac{2}{3}tra(S\Omega^2)\right)+\beta_7\left(S^2\Omega^2+\Omega^2S^2-\frac{2}{3}tra(S^2\Omega^2)\right)\\&\beta_8\left(S\Omega S^2-S^2\Omega S\right)+\beta_9\left(\Omega S\Omega^2-\Omega^2 S\Omega\right)+\beta_{10}\left(\Omega S^2\Omega^2-\Omega^2S^2\Omega\right)\end{aligned} \quad (12)$$

in which the β coefficients may be function of the five independent invariants of S and Ω.

$$\begin{aligned}&N_a=-A_1S+(a\Omega-\Omega a)-A_2\left(aS-Sa-\frac{2}{3}tra(aS)\right)\\&with\qquad N=A_3+A_4(\frac{P_k}{\varepsilon})\end{aligned} \quad (13)$$

The coefficients A_i in this matrix equation depend on the C_i coefficients of the pressure-strain term in the underlying Reynolds stress transport model. Their values are selected here as A_1=1.245, A_2=0, A_3=1.80, and A_4=2.25. S=S_{ij} and Ω=Ω_{ij} denote the non-dimensional strain-rate and vortices tensors, respectively. They are defined as:

$$S_{ij}=\frac{1}{2}\tau_t\left(\frac{\partial U_i}{\partial x_j}+\frac{\partial U_j}{\partial x_i}\right) \quad (14)$$

Please cite this article as: B. Rezaei, A. Safarzade, Numerical modeling of flow field in prismatic compound channels with different floodplain widths, Journal of Applied Research in Water and Wastewater, 3 (2), 2016, 260-270.

$$\Omega_{ij} = \frac{1}{2}\tau_t\left(\frac{\partial U_i}{\partial x_j} - \frac{\partial U_j}{\partial x_i}\right) \quad (15)$$

where the time-scale t_t is given by:

$$\tau_t = \frac{k}{\varepsilon} = \frac{1}{C_\mu \omega} \quad , C_\mu = 0.09 \quad (16)$$

3.4. Introducing ANSYS-CFX

The Computation Fluid Dynamic (CFD) is a capable computer-based tool for simulating the behavior of systems involving flow field, heat transfer and other physical processes. It works by numerically solving the Reynolds Averaged Navier-Stokes equations over a region of interest, with specified boundary conditions. The solution is advanced through space and time to obtain a numerical description of the flow field. The ANSYS-CFX software is a commercial CFD code; it uses the finite volume approach to solve the Reynolds Averaged Navier-Stokes equations.

The advantage of using ANSYS-CFX to other codes is that it offers multiple validated solutions as well as powerful algorithms and discrete techniques, and is also flexible in implantation of boundary condition via user defined FORTRAN subroutines (Morvan et al., 2001; Bonakdari et al., 2011).

4. Simulation of flow field

The height and width of the numerical modeling domain were exactly the same as experimental flume used by Rezaei (2006). Also, an important task was to decide which solver to use. By considering the running time of software and uniform flow condition, the Rigid Lid approach was chosen, which means that the free surface would be fixed at a certain depth by adopting a top boundary with no friction.

4.1. Mesh gridding

In numerical modeling an optimal mesh refinement was pursued, with the aim of optimal computational costs besides maintaining accuracy. Numerical simulations must have a sufficiently fine mesh to resolve the flow field near the main channel and floodplain beds and walls. To study the effect of mesh size on flow modeling, three sets of course, medium and fine mesh size for prismatic compound channel with 400 mm floodplain widths were chosen. The mesh sizes were chosen in such a way that the average refinement ratio was above the recommended minimum value of 1.3 (see Celik *et al*., 2008). Using κ–ε turbulence model and discharge of 40 l/s, the depth-averaged velocity was numerically modeled (see Fig. 3). Fig. 3 indicated that by decreasing cells size accuracy of numerical modeling increase. Also the dispersion diagrams for numerical and experimental data together with an ideal line function of $y=x$ are presented in Figs. 4. As seen in figures by increasing the number of nodes, the points get close to ideal line. It should be noted that the mesh spacing in fine case was chosen in such a way that the dimensionless distance to the wall, y^+(=yu*/ν), was into the range $30<y^+<500$.

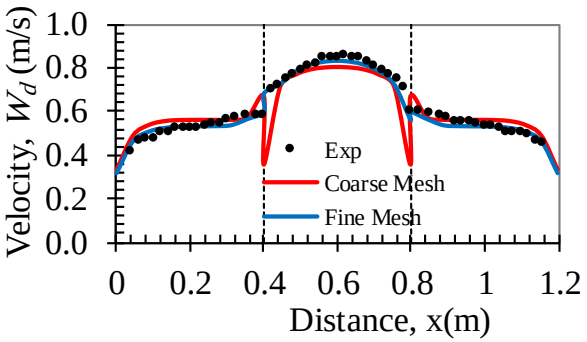

Fig. 3. A comparison between experimental and numerical modeling of depth-averaged velocity for two mesh sizes and discharge of 40 l/s.

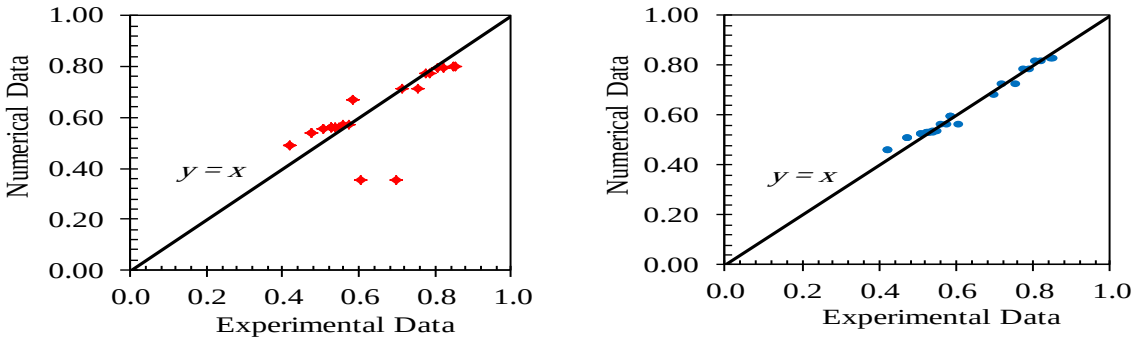

(a) Corse mesh (b) Fine mesh

Fig. 4. Dispersion diagram of velocity for mesh size independency analysis.

The ICEM software is used to get a good grid in numerical model. Since higher accuracy is needed, grids near the water surface, the beds and the interfaces between the main channel and floodplains have been made finer than other parts of flume cross section. Along the flume, because of simple geometry, coarse grids with 0.2 m spaces have been used. Details of gridding are shown plotted in Table 1 and Figs. 5. As

Please cite this article as: B. Rezaei, A. Safarzade, Numerical modeling of flow field in prismatic compound channels with different floodplain widths, Journal of Applied Research in Water and Wastewater, 3 (2), 2016, 260-270.

seen in Table 1 the maximum and minimum size of the elements in the main channel and on the floodplains are 0.006 m and 0.002 m, respectively. To make sure that the flow field in the numerical model is fully developed, 7 m has been added to the flume length.

4.2. Boundary conditions

The solution of flow field was carried out using ANSYS-CFX software with three turbulence models and an iteration procedure with accuracy of 1×10^{-8}. The boundary conditions are as follow: (a) uniform velocity distribution at the flume inlet, (b) hydrostatics pressure condition at the outlet, (c) smooth solid wall with no slip condition in the main channel and on the floodplains walls and beds, and (d) free surface condition on the water surface.

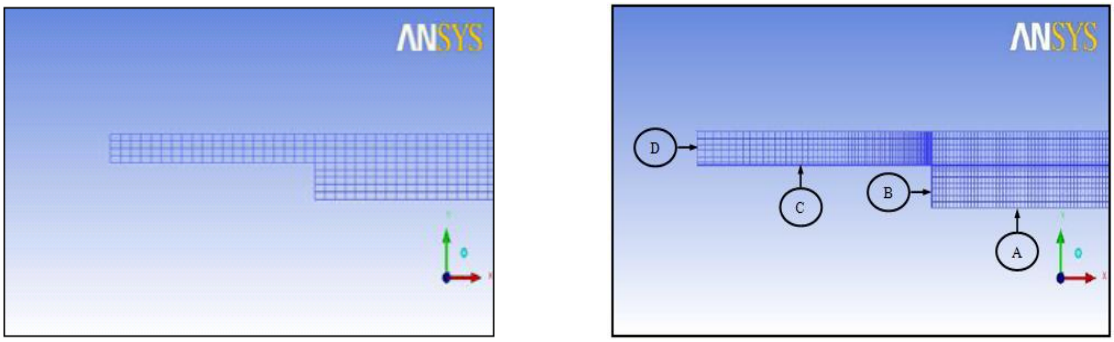

(a) (b)

Fig. 5. Details of gridding in section; (a) coarse mesh, (b) fine mesh.

Table1. Details of gridding for fine mesh.

Element	Number of elements	Max. mesh spacing (m)	Min. mesh spacing (m)
A	70	0.006	0.002
B	10	0.006	0.002
C	Depend on width	0.006	0.002
D	Depend on water depth	0.006	0.002

5. Results

5.1. Velocity distributions

To study the effects of flume geometry on flow field, the stream wise depth-averaged velocity in prismatic compound channel with four different floodplain widths and 12 discharges (Q=12 1/s, 15, 18, 21, 24, 27, 30, 35, 40, 45 and 50 1/s) were modeled using κ–ε, κ–ε EARSM, and Eddy Viscosity Transport turbulence models.

The results of depth averaged-velocity modeled by ANSYS-CFX for two discharges of 24 1/s and 45 l/s are shown in Figs. 6 and 7. As seen in figures the κ–ε and Eddy (e.g. Eddy Viscosity Transport Equation) models are able to predict the depth-averaged velocity distribution, quite well, especially in the main channel. In addition, it is clear that the κ–ε EARSM model cannot predict maximum velocity in the middle of main channel. Figures also show that, in general, by increasing discharges and floodplain widths the discrepancy between the experimental and numerical data decrease. The streamwise velocity predicted by the k-ε and Eddy Viscosity Transport turbulence models are shown in Figs 8(a), 8(b) and Figs. 8(e), 8(f), respectively. These turbulence models do not produce secondary flow, and accordingly its influence is not reflected in stream wise velocity contours. In order to study the effects of floodplain widths and discharges on flow:

$$MAPE = \frac{\sum \left| \frac{W_{d\exp} - W_{dmes}}{W_{\exp}} \right|}{n} \times 100 \quad (17)$$

The mean absolute percentage error (MAPE) of depth average velocity for two discharge of, Q=24 1/s and 45 1/s are also calculated using equation (17) and shown in Table 2. As seen in Table 2 the mean absolute percentage errors for three turbulence models are, usually, less than 8 percent. In which W_{dexp} is experimental point depth-averaged velocity, W_{dmes} is numerical depth-averaged velocity and n is the number of data The streamwise velocity distribution for experimental cases of OPC100-45 and OPC200-45 are also modeled by three turbulence models and shown plotted in Figs. 8. The figures indicate that, all turbulence models are able to predict velocity distribution fairly well. The bulging of the isovels towards the main channel from the floodplain edges in Figs. 8(c) and 8(d) are characteristic of flows where the secondary currents are present. field, the depth-averaged velocity distribution has been normalized. The average velocity in the whole cross section has been used for normalization (see Figs. 9). As seen in the Fig. 9(a), for experimental tests of OPC100-24 and OPC400-24 the normalized velocities on the floodplains are almost the same, while in the main channel the discrepancy between the results of two experimental series are apparent. This fact indicates that for discharge of 24 1/s by increasing floodplain width from 100 mm to 400mm, the interaction between the

Please cite this article as: B. Rezaei, A. Safarzade, Numerical modeling of flow field in prismatic compound channels with different floodplain widths, Journal of Applied Research in Water and Wastewater, 3 (2), 2016, 260-270.

main channel and floodplains increases. As discharge increases from 24 1/s to 45 1/s, the difference between normalized velocity in the main channel and floodplain decrease which means the less interaction between those subsections (see Fig. 9(b)).

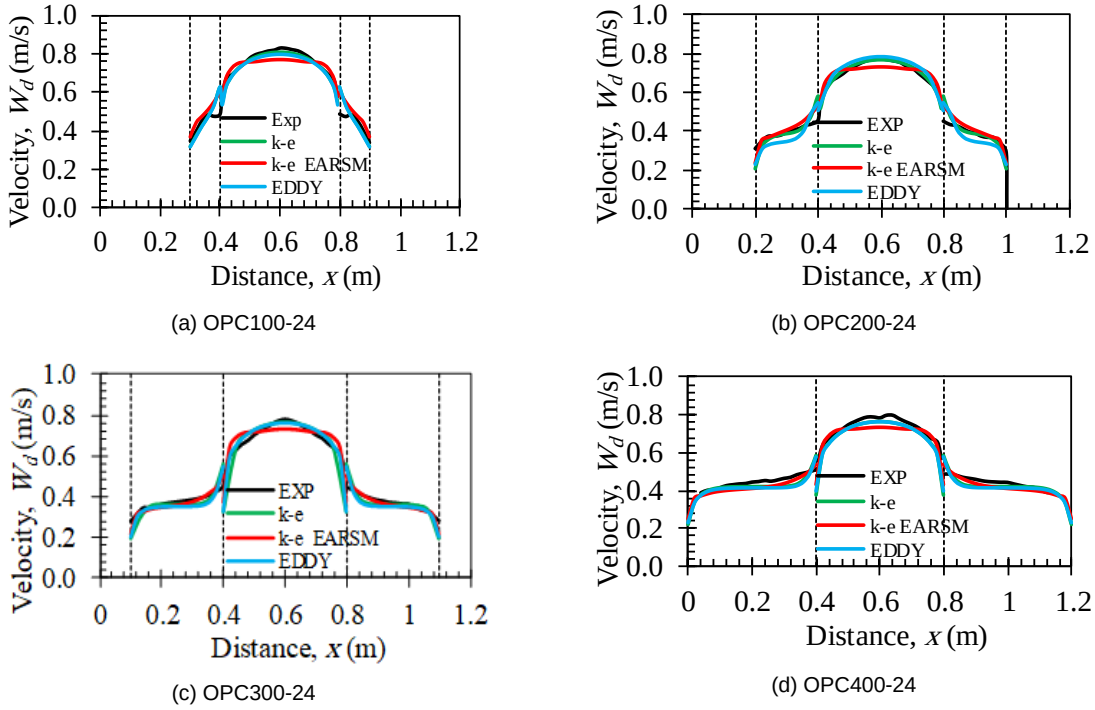

(a) OPC100-24 (b) OPC200-24

(c) OPC300-24 (d) OPC400-24

Fig. 6. Depth–averaged velocity distribution in prismatic compound channels with different floodplain widths and Q = 24 l/s.

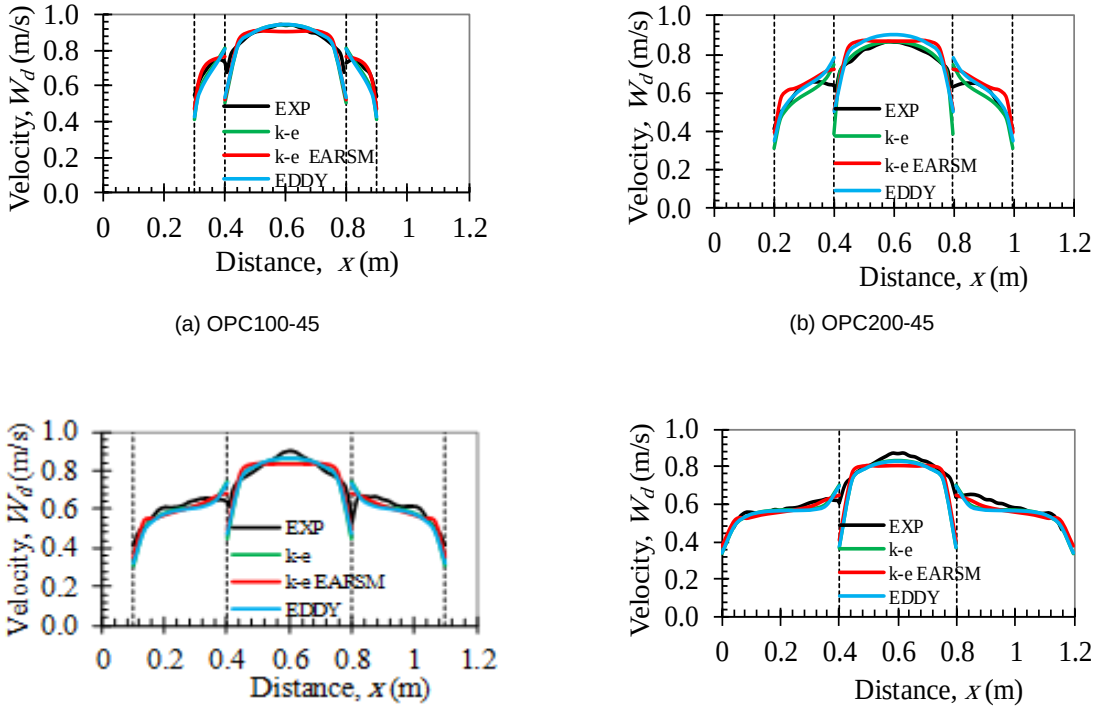

(a) OPC100-45 (b) OPC200-45

(c) OPC300-45 (d) OPC400-45

Fig. 7. Depth–averaged velocity distribution in prismatic compound channels with different floodplain widths and Q = 45 l/s.

Please cite this article as: B. Rezaei, A. Safarzade, Numerical modeling of flow field in prismatic compound channels with different floodplain widths, Journal of Applied Research in Water and Wastewater, 3 (2), 2016, 260-270.

Table 2. The mean absolute percentage error (MAPE) of depth average velocity for three turbulence model; a) *Q*=24 l/s, b) *Q*=45 l/s.

a) *Q*=24 l/s

Experimental	κ−ε	κ−ε EARSM	Eddy
OPC100	5.18	6.65	5.91
OPC200	5.15	6.21	13.68
OPC400	7.23	6.91	7.89

b) *Q*=45 l/s

Experimental	κ−ε	κ−ε EARSM	Eddy
OPC100	5.22	3.52	5.80
OPC200	5.93	4.23	6.34
OPC400	5.00	4.77	5.28

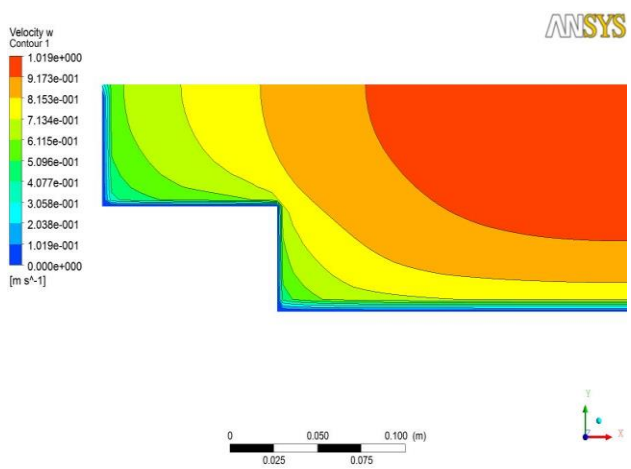

(a) OPC100-45 (κ−ε model)

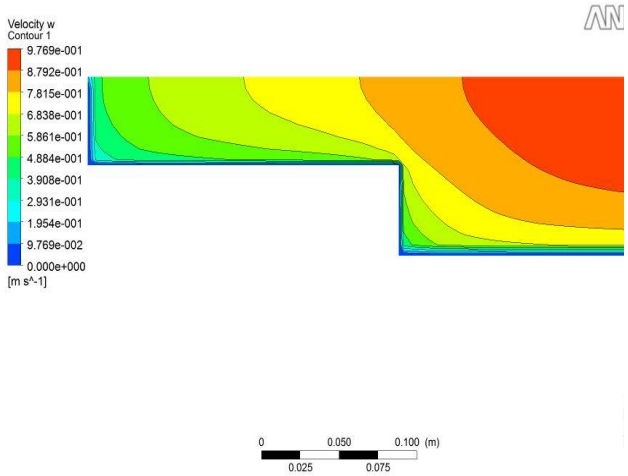

(b) OPC200-45 (κ−ε model)

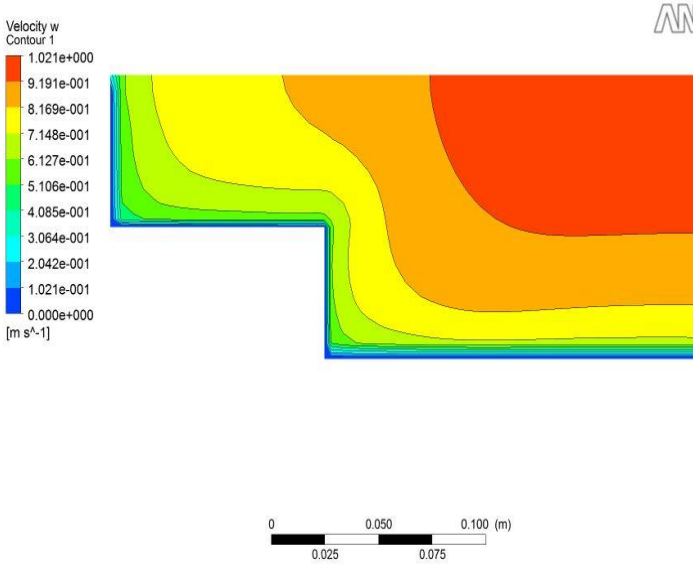

(c) OPC100-45 κ−ε EARSM model)

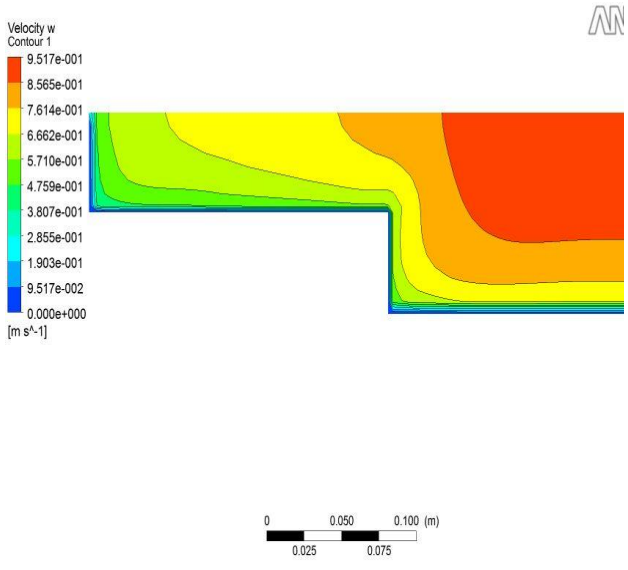

(d) OPC200-45 (κ−ε EARSM model)

Please cite this article as: B. Rezaei, A. Safarzade, Numerical modeling of flow field in prismatic compound channels with different floodplain widths, Journal of Applied Research in Water and Wastewater, 3 (2), 2016, 260-270.

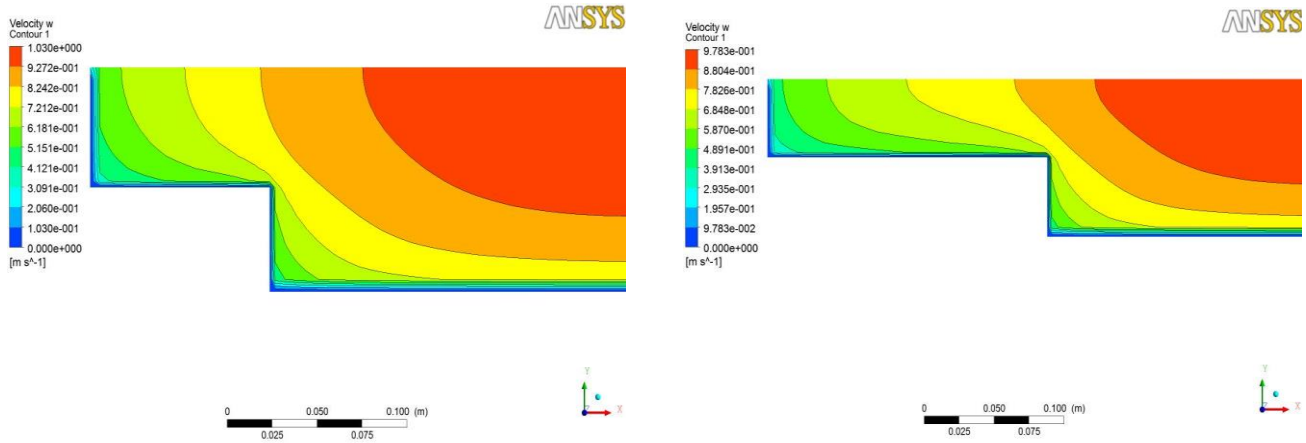

(e) OPC100-45 (Eddy model)

(f) OPC200-45 (Eddy model)

Fig. 8. Streamwise velocity Distribution simulated using turbulence models for experimental series of OPC100-45 and OPC200-45 (a, b) $\mathcal{K}-\mathcal{E}$, (c, d) $\mathcal{K}-\mathcal{E}$ EARSM, and (e, f) Eddy Viscosity Transport Equation.

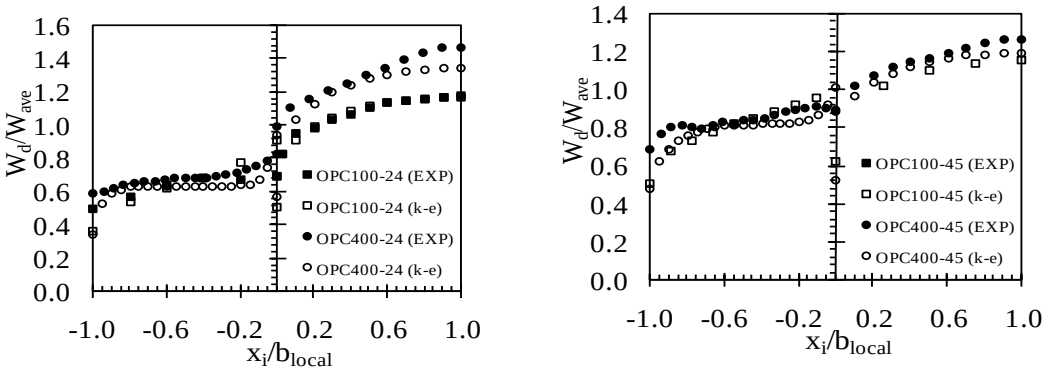

(a)

(b)

Fig. 9. A comparison between experimental and numerical normalized depth-averaged velocity for two experimental series of OPC100 and OPC400; (a) Q=24 l/s, (b) Q=45 l/s

5.2. Boundary shear stress distributions

Boundary shear stress distribution is another important parameter in river engineering when studying sediment transport and riverbank protection. It also is important for river modelers when calibrating a mathematical model, which commonly requires numerical values of resistance coefficients. The boundary shear stress distributions calculated using the three turbulence models. The results of numerical modeling were then compared with experimental data (see Figs. 10). Figs. show that; (a) all three turbulence models always underestimate boundary shear stress on the floodplain, (b) discrepancy between numerical results and experimental data near the interface of main channel and floodplain, significantly, increase, (c) the *k-ε* turbulence model underestimates shear stress in the main channel, while the EDDY turbulence model overestimates it, (e) similar to depth-averaged velocity distributions, the *k-ε* EARSM turbulence model is not able to predict maximum shear stress in the main channel, (f) the *k-ε* EARSM model predicts two picks near the main channel walls which indicates the presence of strong secondary flow cells in this part of the flume. The mean absolute percentage error (MAPE) of shear stress for two discharge of, *Q*=24 l/s and 45 l/s are also calculated and shown in Table 3. As seen in the table, among those turbulence models, the κ–ε EARSM model has the minimum MAPE also by increasing floodplain widths and flow discharges the difference between the experimental and numerical data decrease.

5.3. Secondary flow

The secondary flow patterns for two floodplain widths (300 mm and 400 mm) and discharges *Q*= 24 1/s and 45 l/s are simulated using $\kappa-\varepsilon$ EARSM turbulence model (see Fig. 11). The figures clearly show the effects of geometry and discharge on secondary flow pattern. For the compound channel with 300 mm and 400 mm floodplain widths and discharge of 24 1/s, presence of one strong secondary flow cell in the main channel are clear, as the discharge raise to 45 1/s the number of secondary flow circulations increase to three cells, one cell in the main channel and two strong secondary flow cells near the interface between the main channel and floodplains. This emphasizes that two secondary flow cells interacted near the interface is responsible for pushing upwards particles with smaller velocities, causing the inflection of the isovel lines and increasing depth-averaged velocity and shear stress near the main channel walls.

Please cite this article as: B. Rezaei, A. Safarzade, Numerical modeling of flow field in prismatic compound channels with different floodplain widths, Journal of Applied Research in Water and Wastewater, 3 (2), 2016, 260-270.

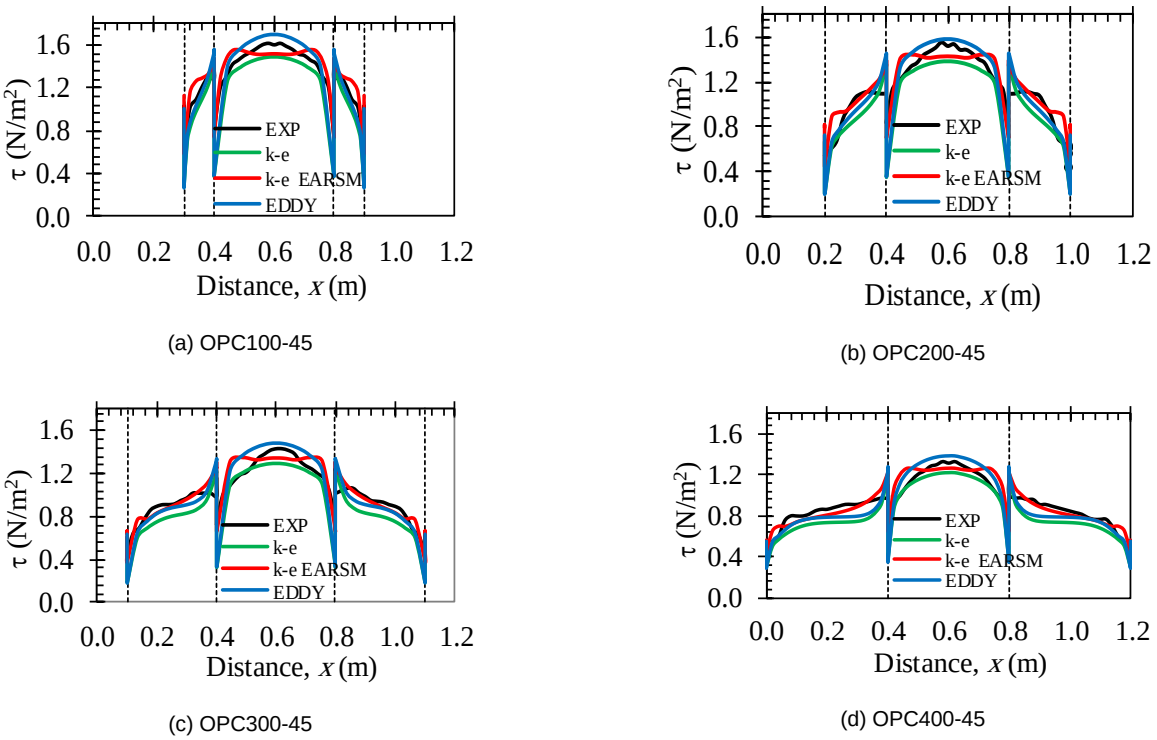

(a) OPC100-45

(b) OPC200-45

(c) OPC300-45

(d) OPC400-45

Fig. 10. Shear stress distribution in prismatic compound channel with different floodplain widths and *Q* = 45 l/s.

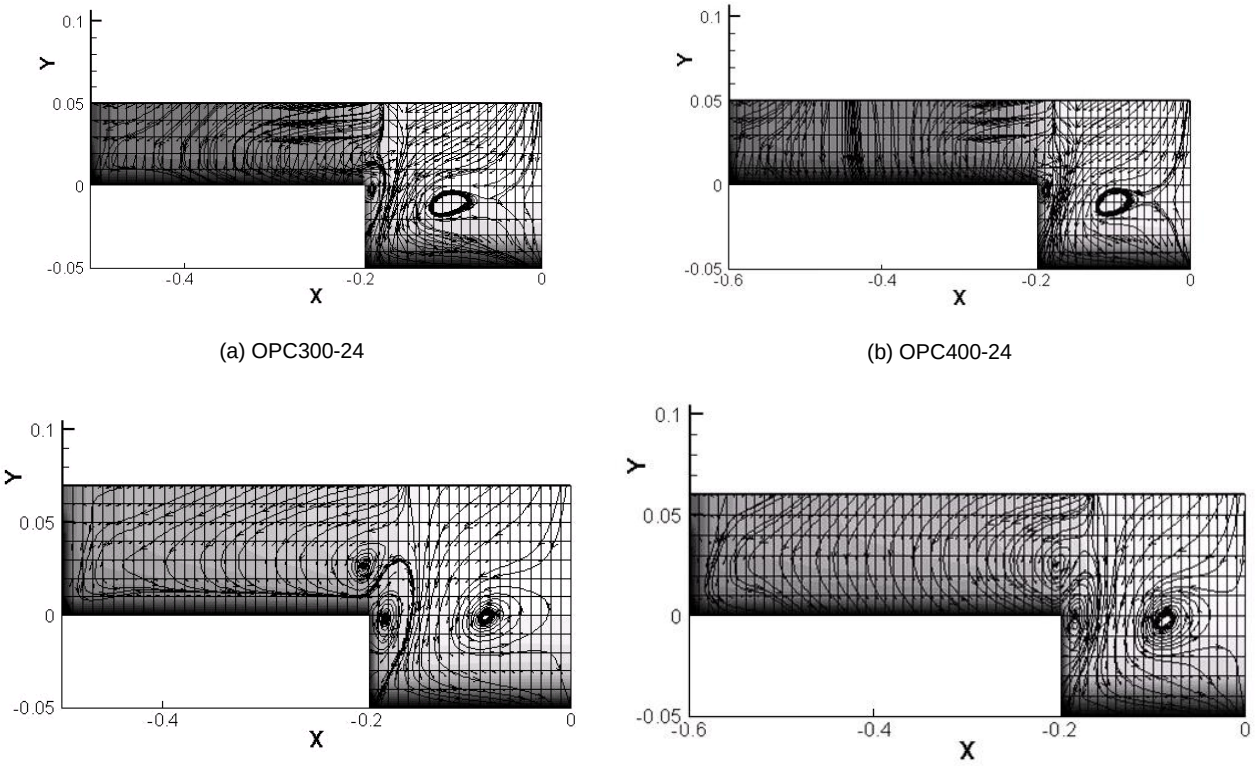

(a) OPC300-24

(b) OPC400-24

(c) OPC300-45

(d) OPC400-45

Fig. 11. Secondary current circulations predicted using κ–ε EARSM turbulence model in prismatic compound channels for two discharges of 24 l/s and 45 l/s.

Please cite this article as: B. Rezaei, A. Safarzade, Numerical modeling of flow field in prismatic compound channels with different floodplain widths, Journal of Applied Research in Water and Wastewater, 3 (2), 2016, 260-270.

Table 3. The mean absolute percentage error (MAPE) of shear stress distribution for three turbulence model; a) *Q*=24 l/s, b) *Q*=45 l/s.

a) *Q*=24 l/s

Experimental	κ−ε	κ−ε EARSM	Eddy
OPC100	17.87	12.17	22.23
OPC200	14.94	10.48	33.55
OPC400	19.50	12.51	18.77

b) *Q*=45 l/s

Experimental	κ−ε	κ−ε EARSM	Eddy
OPC100	16.81	6.77	19.88
OPC200	16.09	8.88	16.50
OPC400	14.36	6.69	13.42

6. Conclusions

The velocity and boundary shear stress distributions in prismatic compound channels with different floodplain widths were numerical simulated using three turbulence models, including the κ–ε, κ–ε EARSM and Eddy Viscosity Transport turbulence models. The results of numerical modeling were then compared with the experimental data.

1. The depth-averaged velocity distribution predicted using three turbulence models are in good agreement with the experimental data. Comparing to the κ–ε and κ–ε EARSM models, the Eddy Viscosity Transport Equation turbulence model can predict the depth-averaged velocity reasonably well, especially in the main channel. Also by increasing the floodplain width, the divergence between numerical modeling and the experimental data decrease.
2. To compare with depth-averaged velocity, the shear stress distribution predicted by the κ–ε, κ–ε EARSM and Eddy Viscosity Transport turbulence models are in less agreement with the experimental data.
3. By increasing flow discharge (water depth) and floodplains width, the accuracy of three turbulence models improves.
4. Among those three turbulence models, only the *k*-*e* EARSM are able to predict secondary flow cells in the main channel and floodplains. As a result of interaction between the secondary flow cells, the *k*-*e* EARSM turbulence model shows two local peaks in shear stress distributions near the main channel walls.

References

Beaman F., Large eddy simulation of open channel flows for conveyance estimation, PhD Thesis, Nottingham University, UK (2010).

Bonakdari H., Baghalian S., Nazari F., Fazli M., Numerical analysis and prediction of the velocity field in curved channel using artificial neural network and genetic algorithm, Engineering Applications of Computation Fluid Mechanics 5(2011) 384-396.

Bousmar D., Flow modeling in compound channels – Momentum transfer between main channel and prismatic or non-prismatic floodplains, PhD Thesis, Universite Catholique de Louvain, Belgium (2002).

Celik I.B., Ghia U., Roache P.J., Procedure for Estimation and Reporting of Uncertainty Due to Discretization in CFD Applications, Journal of Fluids Engineering 130 (2008) 1-4.

Cokljat D., Turbulence models for non-circular ducts and channels, PhD Thesis, City University London, UK (1993).

Okljat D., Younis B., Second order closure study of open-channel flow, Journal of Hydraulic Engineering 121 (1995) 773-788.

Ikeda S., Role of lateral eddies in sediment transport and channel formation, River Sedimentation, Jayawardena, Lee and Wang, eds., Balkema Rotterdam, (1999) 195-203.

Jing H., Guo Y., Li C., Zhang J., Three-dimensional numerical simulation of compound meandering open channel flow by Reynolds stress model, International Journal for Numerical Method in Fluid 59 (2009) 927-943.

Kang H., Choi S.U., 3D Numerical simulation of compound open-channel flow with vegetated floodplains by Reynolds stress model, KSCE Journal of Civil Engineering 9 (2005) 7-11.

Launder B.E., Spalding D.B., The numerical computation of turbulent flows, Computer Method and Application and Engineering 3 (1974) 269-289.

Menter F.R., Eddy viscosity transport equations and their relation to the k-ε model, Journal of Fluids Engineering 119 (1997) 876-884.

Morvan N., Pender G., Ervine D.A., Three-Dimensional hydrodynamics of meandering compound channels, Journal of Hydraulic Engineering 128 (2001) 674-682.

Myers W.R.C., Momentum transfer in a compound channel, Journal of Hydraulic Research, 16 (1978) 139-150.

Naot D., Nezu I., Nakagava H., Calculation of compound open channel flow, Journal of Hydraulic Engineering 119 (1993) 1418-1426.

Nezu I., Nakagawa H., Turbulence in open-channel flows, IAHR Monograph Series, A.A., Balkema, Rotterdam, Netherlands, (1993).

Pezzinga G., Velocity distribution in compound channel flows by numerical modeling, Journal of Hydraulic Engineering 120 (1994) 1176-1197.

Rezaei B., Overbank flow in compound channels with prismatic and non-prismatic floodplains, PhD Thesis, Birmingham University, UK (2006).

Please cite this article as: B. Rezaei, A. Safarzade, Numerical modeling of flow field in prismatic compound channels with different floodplain widths, Journal of Applied Research in Water and Wastewater, 3 (2), 2016, 260-270.

Rezaei B., Knight D.W., Overbank flow in compound channels with nonprismatic floodplains, Journal of Hydraulic Engineering 137 (2011) 815-824.

Sellin R.H.J., A laboratory investigation into the interaction between the flow in the channel of a river and that over its floodplain, La Houille Blanche 7 (1964) 793-802.

Shiono K., Knight D.W., Turbulent open-channel flows with variable depth across the channel, Journal of Fluid Mechanics, 222 (1991) 617-646.

Tominaga A., Nezu I., Turbulent structure in compound open-channel flows, Journal of Hydraulic Engineering 117 (1991) 21–41.

Wallin S., Engineering turbulence modeling for CFD with a focus on explicit algebraic Reynolds stress models, PhD Thesis, Norsted Tryckeri AB, Stockholm, Sweden (2000).

Wallin S., Johansson A., A complete explicit algebraic Reynolds stress model for incompressible and compressible flows, Journal of Fluid Mechanics 403 (2000) 89-132.

Wormleaton P.R., Floodplain secondary circulation as a mechanism for flow and shear stress redistribution in straight compound channels, Chap. 28, Coherent Flow Structures in Open Channels, Editors Ashworth, Bennett, Best, McClelland, J Wiley, (1996), 581-608.

Wright N.G., Crosseley A.J., Morvan H.P., Stoesser T., Detailed validation of CFD for flows in straight channels, River Flow 2004, Naples, Italy, (2004) 1041-1048.

Please cite this article as: B. Rezaei, A. Safarzade, Numerical modeling of flow field in prismatic compound channels with different floodplain widths, Journal of Applied Research in Water and Wastewater, 3 (2), 2016, 260-270.